

Production of machined gypsum/polymer blocks for use in three-dimensional milling systems and later conversion to hydroxyapatite

A. L. M. S. Moreira¹, T. I. D. Santos¹, N. C. Olivier¹, A. C. S. Dantas^{1*}

¹Universidade Federal do Vale do São Francisco, Programa de Pós-Graduação em Ciências dos Materiais, Juazeiro, BA, Brazil

Abstract

The chemical conversion of gypsum into synthetic hydroxyapatite is an attractive approach to enhance the value of gypsum, a low-cost material, which can be discreetly implanted. The addition of biopolymers improves the resistance of the materials both before and after conversion. In this study, hydroxyapatite was produced from gypsum using a fixed water-to-gypsum ratio (w/g) of 0.7, along with gypsum/polymer composites. The polymers employed were polyhydroxybutyrate (PHB) and polyvinyl acetate (PVAc) at various mass ratios. Two methods were used to create the bodies: molding the paste and subtractive manufacturing. Mechanical compression tests were conducted both pre- and post-conversion to evaluate the impact of the conversion on material resistance and to compare it with the strength of subtractive manufacturing composites. For the gypsum/PHB composite, the best result was achieved at a 1% polymer concentration, yielding a resistance of 9.1 ± 0.4 MPa, while for gypsum/PVAc, a compressive strength of 9.3 ± 0.3 MPa was obtained at a 2% polymer concentration.

Keywords: gypsum, hydroxyapatite, machinability, subtractive manufacturing.

INTRODUCTION

β -gypsum is a low-cost material with good workability. Its primary application is in the civil construction industry, but it can also be alternatively used for creating molds [1] or processed and transformed into hydroxyapatite [2]. Gypsum obtained from the region of Araripe-PE, Brazil, exhibits high purity, with more than 99% calcium sulfate [2]. Alternatively, subtractive manufacturing processes aided by computer numerical control (CNC) [3], such as turning and milling, can be used to shape the material satisfactorily. These advanced manufacturing technologies enable the creation of real three-dimensional models starting from a virtual design [4].

In this study, polyhydroxybutyrate (PHB) was utilized as a biodegradable additive [5, 6], and polyvinyl acetate (PVAc) [7] served as an easily removable additive. The addition of these polymers aimed to improve the mechanical properties of gypsum and reduce its porosity, making machining more feasible. Compression tests were conducted to characterize the mechanical properties of the specimens and evaluate the loss of mechanical properties after the machining process [8]. Ceramic materials, in general, present challenges when it comes to machining due to their inherent characteristics, including high hardness and fragility [9].

The objectives of this study were as follows: a) evaluation of the changes in the mechanical properties of the gypsum matrix induced by the addition of different concentrations of polymers before and after chemical conversion into hydroxyapatite; and b) investigation of the machinability of

β -gypsum by evaluating the forces involved in the turning machining process under various cutting configurations.

MATERIALS AND METHODS

Sample production occurred through two different approaches. Stage 1: samples were produced using cylindrical molds, with one group intended for measuring machining forces and another for assessing physical and mechanical properties. Stage 2: a prismatic body was manufactured, and samples were machined using a CNC machining center. Part of this group was allocated for measuring mechanical and physical properties, while another part was converted into hydroxyapatite, followed by structural characterization and property measurements. For turning experiments, a lathe (MS 2206 Gold, Nardini) was employed, and for milling, a CNC vertical machining center (D600, Romi) powered by a 15 kW motor with a speed range of 10000 rpm was utilized. The gypsum used in the experiments was commercial β type (80% to 95% pure) $\text{CaSO}_4 \cdot 0.5\text{H}_2\text{O}$ (Gesso Miner. Ind., Araripe, Pernambuco State, Brazil). The preparation of the gypsum paste followed the guidelines of the NBR 12129 standard [2]. A water-to-gypsum ratio (w/g) of 0.7 was chosen due to the high workability of the paste after the addition of polymers [2]. For the experiments involving cylindrical molds, the molds had average dimensions of $h=100$ mm \times $\phi=52$ mm (for machinability tests) and $h=20$ mm \times $\phi=10$ mm (for compression tests). The demolding time was approximately 48 h, and the tests were conducted after a curing period of 360 h post-demolding. Prismatic specimens, with dimensions of $h=65$ mm \times $l=50$ mm \times $c=150$ mm, were created for subtractive manufacturing and later machined into 16 cylindrical samples ($h=20$ mm \times $\phi=10$ mm). Among these machined cylindrical specimens, 6

*engmec.andremoura@gmail.com

 <https://orcid.org/0000-0002-2036-8182>

samples were earmarked for the conversion of gypsum and composites into hydroxyapatite.

The compressive strength test of the bodies was conducted using a universal mechanical testing machine (DL 1000, Emic), a load cell with a capacity of 20 kN, and a test speed of 2 mm/min. Data acquisition and storage were managed using software (Tesc). Compressive strength was defined as the maximum stress that a body can endure during the testing process. The compression stress was calculated as follows:

$$\sigma_c = F_m / A_s \quad (\text{A})$$

where σ_c is the compressive strength (MPa), F_m is the compressive load (N), and A_s is the surface area (mm_2).

The machinability was evaluated by measuring the machining forces by the turning process. Machining forces were measured in the feed direction (\vec{F}_f , axial force) and cutting force (\vec{F}_{ig} , tangential force), which are the active forces \vec{F}_T in machining, according to²⁷:

$$\vec{F}_T = \vec{F}_{ig} + \vec{F}_f \quad (\text{B})$$

Each cutting setup (defined by cutting depth x feed rate) was repeated three times to obtain an average measurement value for β -gypsum. The rotational speed of the workpiece was consistently set at 750 rpm for all tests. The machining tests were conducted using the lathe in a cylindrical turning process applied to the samples. Throughout the tests, a bar-type tool made of high-speed steel with specific angles, including a 7° back rake angle, 19° end-cutting edge angle, and 8° main angle, was employed. This tool was positioned at a 90° angle relative to the transverse axis of the workpiece. The machining parameters for the cutting tests included a feed rate of 0.08, 0.12, 0.20, and 0.25 mm/rev and cutting depths of 0.5, 1.0, and 1.5 mm. The cutting speed was calculated using the following formula:

$$V_c = \frac{\pi \cdot d \cdot n}{1000} \quad (\text{C})$$

where V_c is the cutting speed (m/min), d is the diameter (mm), and n is the spindle speed (rpm). The cutting forces were measured using a load cell in conjunction with a data acquisition system (ADS2000, Lynx), which included a signal conditioner (AI2164/8) and a controller board (AC2122VB), along with software (AqDados and AqDAnalysis). The acquisition mode was set to 'simple', with a requested sample frequency of 50 Hz, and a maximum test duration of 1 min. Two input channels of the data acquisition system were employed: one for measuring the force in the cutting direction and the other for measuring the force in the feed direction.

The chemical conversion of gypsum specimens and composites into hydroxyapatite followed the methodology proposed by Barbosa et al. [2]. This method involved a wet process, utilizing materials containing the ions of interest (Ca^{2+} and PO_4^{3-}), and maintaining them in the presence of a

hydrothermal solution under ambient pressure. The reagents used in the experiment included di-basic ammonium phosphate $[(\text{NH}_4)_2\text{HPO}_4]$ with a concentration of 0.5 mol.L⁻¹, which was held at 100 °C for 51 h. Ammonium hydroxide (NH_4OH) was used for pH control, maintaining it within the range of 6.0 to 9.0. Both reagents were of analytical grade. After the reaction, the specimens were washed with deionized water until a neutral pH was achieved and then dried in an oven at 50 °C. The samples were characterized using X-ray diffraction (XRD, MiniFlex 600, Rigaku; radiation $\text{CuK}\alpha$) and scanning electron microscopy (SEM, VEGA 3XM, Tescan) coupled with an energy dispersive spectroscope (EDS). For the Fourier transform infrared spectroscopy (FTIR, Spectrum Two, PerkinElmer), the samples were mixed with 0.3 g of KBr and compressed into pellet form, which were then analyzed using the transmittance technique in the range of 4000 to 400 cm^{-1} .

RESULTS AND DISCUSSION

The microstructure of the dihydrate gypsum particles is depicted in Fig. 1a, displaying a predominant prismatic needle shape consistent with the standard morphology of calcium sulfate dihydrate [10]. In Fig. 1b, the EDS spectrum reveals the presence of chemical elements in the samples: calcium, oxygen, and sulfur, which corresponded to the chemical composition of calcium sulfate, confirming the high purity of the dihydrate. The X-ray diffraction pattern (Fig. 1c) exhibits high-intensity peaks at $2\theta = 11.68^\circ$, 20.76° , and 29.17° , along with lower-intensity peaks at $2\theta = 23.39^\circ$, 28.13° , 31.10° , and 33.36° . These peaks aligned with those documented in the Inorganic Crystal Structure Database (ICSD), as indicated by the ICSD 27221 peaks for gypsum. Fig. 1c also presents a low-intensity peak at 25.33° (indicated with *), which did not have a corresponding entry in ICSD 27221. This peak was associated with anhydrite III ($\text{CaSO}_4 \cdot \xi \text{H}_2\text{O}$) attributed to high calcination temperatures [2]. However, it is worth noting that anhydrite III possesses a hydrophilic character and tends to rapidly transform into hemihydrate [2].

Machinability was evaluated as a comparative numerical value [11], using gypsum as the standard material. In Fig. 2, the forces related to the machining process of gypsum at three different depths of cut are illustrated. It was evident that the greater the depth of cut, the higher the total machining force for the same feed speed. An increase in the cutting depth led to a more pronounced rise in force values. For a depth of cut (a_p) of 0.5 mm, lower force values were observed, with the cutting and resultant forces reaching approximately 1 N only at a feed rate (f) of 0.25 mm/rev. The feed force remained close to zero. At $a_p = 1.0$ mm, there was a slight increase in machining force with an increase in cutting speed, and for $a_p = 1.5$ mm, a linear increase in both cutting and resultant forces with an increase in feed rate was observed. For this cutting depth, the cutting forces reached 2.5 N at a feed rate of 0.25 mm/rev. This behavior aligned with another study [12], which demonstrated an increase in power consumption

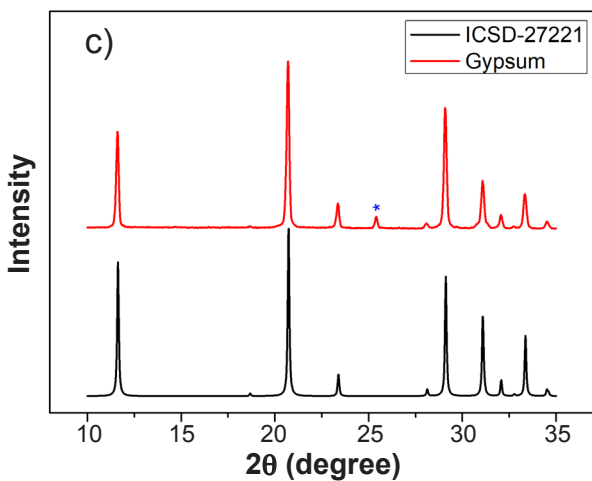
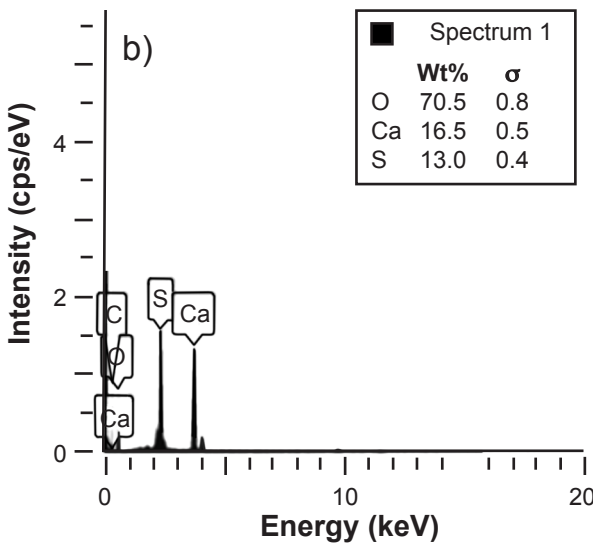
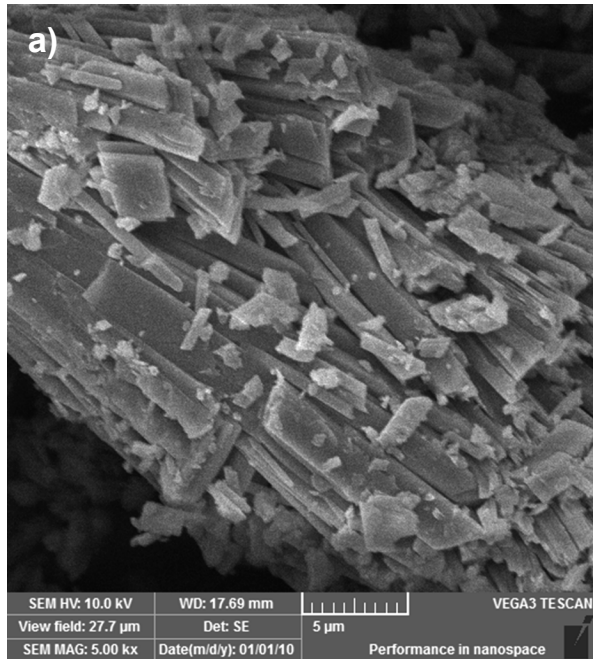


Figure 1: SEM micrograph (a), EDS spectrum (b), and XRD pattern (c) of dehydrated gypsum powder.

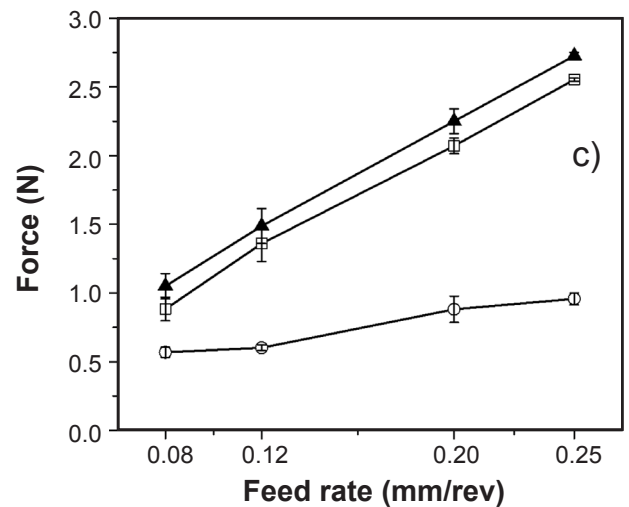
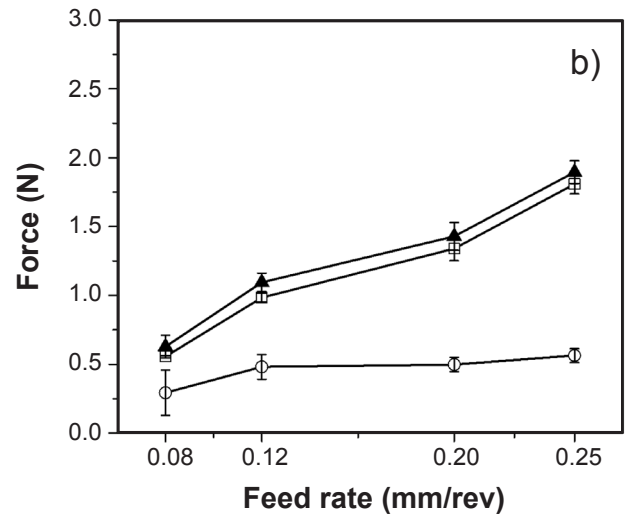
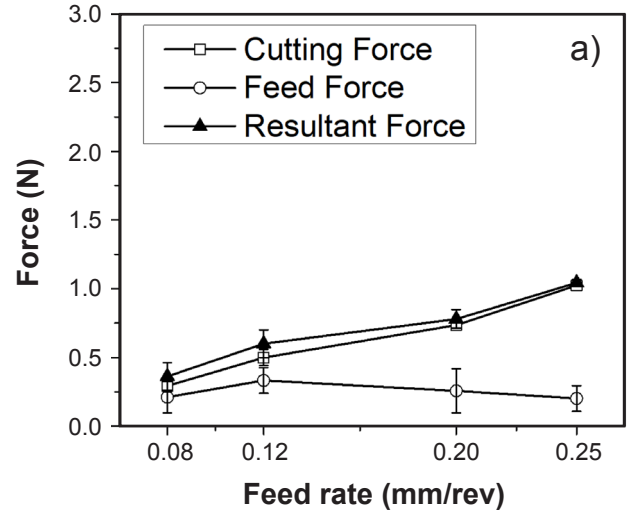


Figure 2: Experimental gypsum cutting forces as a function of feed rate for different depths of cut (a_p) of 0.5 mm (a), 1.0 mm (b), and 1.5 mm (c).

by the machining process with higher feed speeds and/or cutting depths. Across all tests, it was noticeable that the cutting force had a more pronounced influence on the total machining force than the feed force.

In Figs. 3a to 3c, the relationship between cutting forces and feed rate for various cutting depths and different amounts of PVAc in the composite is depicted. When analyzing each composite individually, it became evident that they exhibited the same behavior: as the cutting depth and/or feed rate increased, the machining force also increased. The composites exhibited higher machining force values compared to those measured for pure gypsum, with an increase of up to 73% in cutting force observed for the composite containing 5% PVAc, machined with a depth of cut (a_p) of 0.5 mm and a feed rate (f) of 0.08 mm/rev. Specifically, composites with a concentration of 5% PVAc displayed the highest cutting force values. In all configurations, the force required to machine the composites exceeded that required for gypsum, with increases ranging from 20% to 73% and reaching a peak value of $F_t=3.38$ N (at $a_p=1.5$ mm and $f=0.25$ mm/rev). The results for gypsum/PHB composites, depicted in Figs. 3d to 3f, with mass concentrations of 1%, 2%, and 5% of PHB, revealed F_t values closely aligned with those measured for pure gypsum. This indicated that the cutting forces were not significantly influenced by the amount of PHB added to the composites.

Fig. 4a presents the data obtained from the compression tests conducted on gypsum and composites with different polymer concentrations. It was evident that the addition of PHB polymer to the ceramic matrix led to an increase in compressive strength (σ_c) up to a mass concentration of 1%,

resulting in a gain of 9.85% in σ_c . However, higher quantities of PHB resulted in a decrease in compressive strength values. This effect can be attributed to a reduction in the density of the composite compared to pure gypsum due to the addition of the polymer, which in turn increases porosity [2]. Similarly, the addition of PVAc exhibited a similar behavior (Fig. 4a). However, the composite with 2% PVAc showed the highest increase in maximum compressive strength, with a 12.25% improvement compared to gypsum. It is worth noting that higher quantities of PVAc in the composite disrupt the hydrogen bonds between water molecules, leading to a reduction in their mechanical resistance [13].

The PVAc content in the composites has a significant impact on the kinetics of water loss, which directly influences the crystallization process of the composite, leading to a reduction in the size of the crystallites [14]. However, both PHB and PVAc caused an increase in porosity within the ceramic matrix as their contents increased (Fig. 4b). Consequently, a decrease in compressive strength (σ_c) was observed for higher polymer content. Porosity is closely tied to density (grain packing), just as the mechanical resistance to compression relies directly on the density of the composite [2]. Pores within ceramic materials diminish the cross-sectional area over which the load is applied, compromising the material's ability to withstand stress [16]. For the composite containing 2% PVAc, an enhancement in mechanical resistance to compression was noted. This

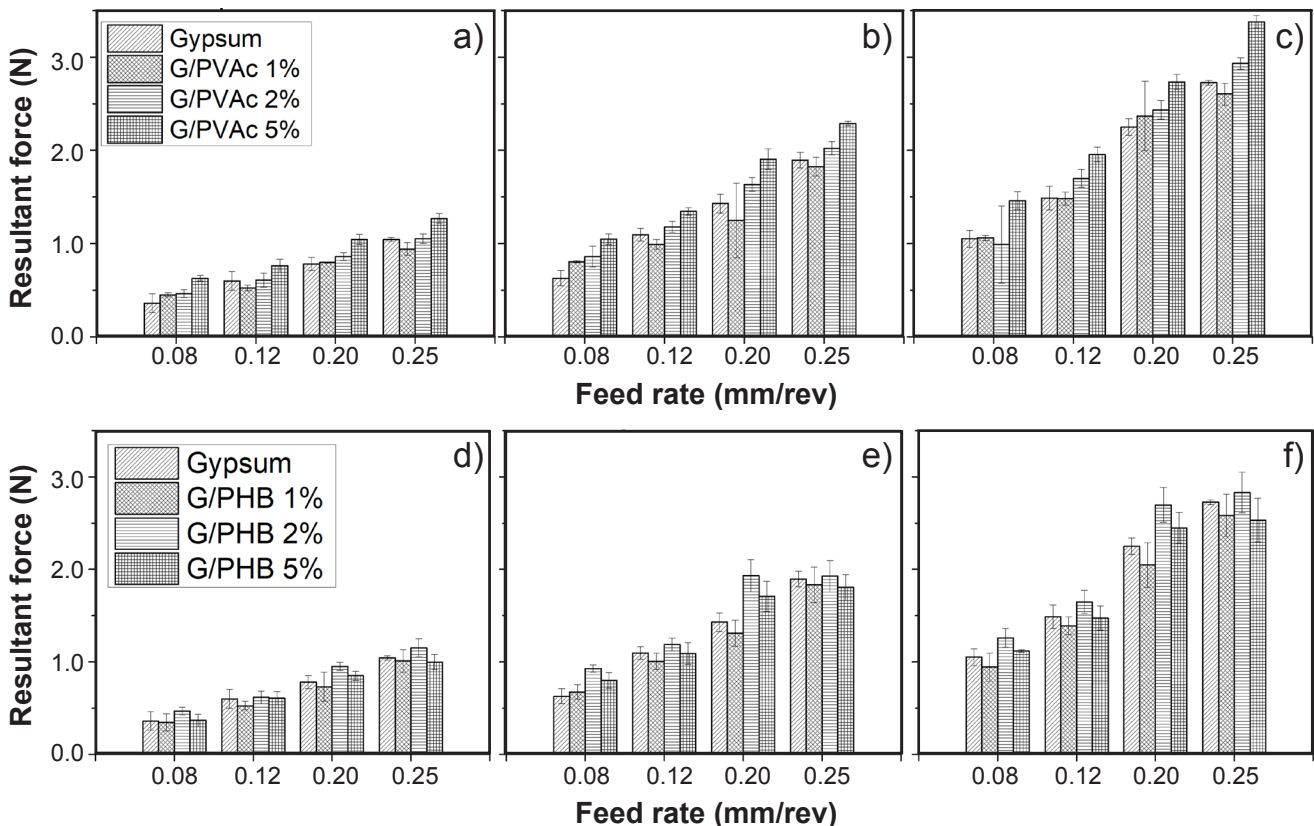


Figure 3: Cutting forces of gypsum/PVAc (a,b,c) and gypsum/PHB (d,e,f) composites as a function of feed rate for different depths of cut (a_p) of 0.5 mm (a,d), 1.0 mm (b,e), and 1.5 mm (c,f).

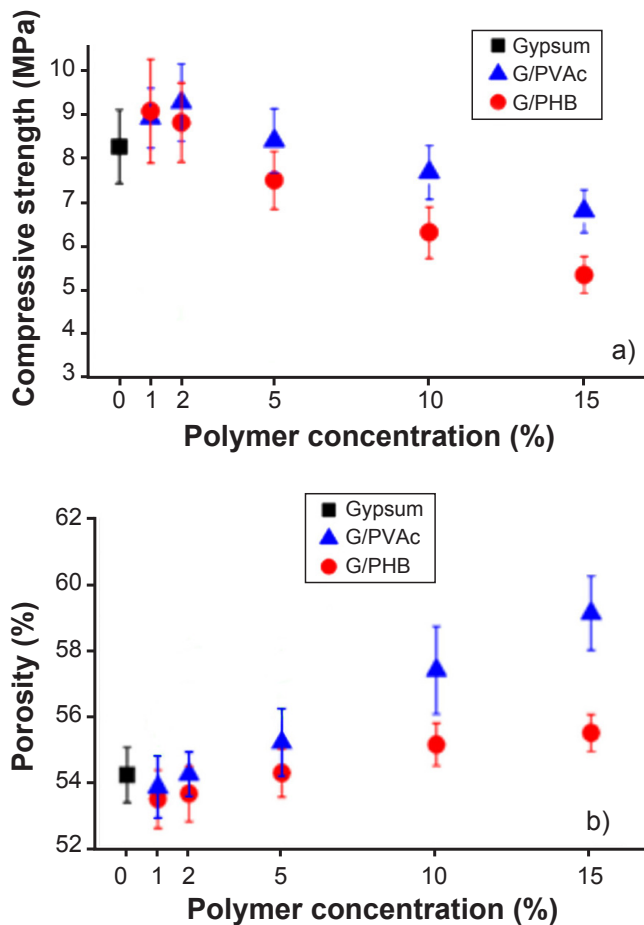


Figure 4: Compressive strength (a) and porosity (b) vs. polymer concentration of molded samples of gypsum and composites.

improvement can be attributed to increased adhesion between the crystals, as suggested by Su et al. [15]. Such enhanced adhesion promoted better stress distribution throughout the material when polymeric additives were introduced into the gypsum matrix. Notably, Fig. 4b shows a continuous increase in porosity starting from a 5% PVAc content in the material, leading to reduced density and consequently diminished mechanical resistance.

Mechanical properties of the machined samples were assessed to examine the impact of the machining process on the mechanical characteristics of both gypsum and gypsum/polymer composites (Fig. 5). It was notable that the mechanical properties of all machined samples were inferior to those of molded samples. This underscored the detrimental effect of the machining process on the mechanical properties of ceramic bodies, likely attributed to the generation of micro-cracks within the bodies as a result of tool vibrations during processing. PVAc composites with mass concentrations of 2% and 5% displayed no significant difference in compressive strength when compared to the pure gypsum sample. Conversely, the addition of PHB to the ceramic matrix in this context led to a reduction in compressive strength. This decline in compressive strength can be attributed to the highly porous structure of the

material, which offered minimal internal support against forces during the machining process [17]. As highlighted by Denkena et al. [18], intense local stress fields occur during the machining of ceramic materials, resulting in a thin surface layer subjected to high stresses that can induce crack formation. This surface damage can ultimately degrade the material's resistance. In Fig. 5, it is evident that the addition of polymers to the ceramic matrix increased the porosity of the composites, leading to a decrease in compressive strength. However, even with the increased porosity, samples with 2% and 5% PVAc maintained their compressive strength, which was not the case with the composite containing 1% PVAc, which exhibited an 18.1% reduction compared to pure gypsum.

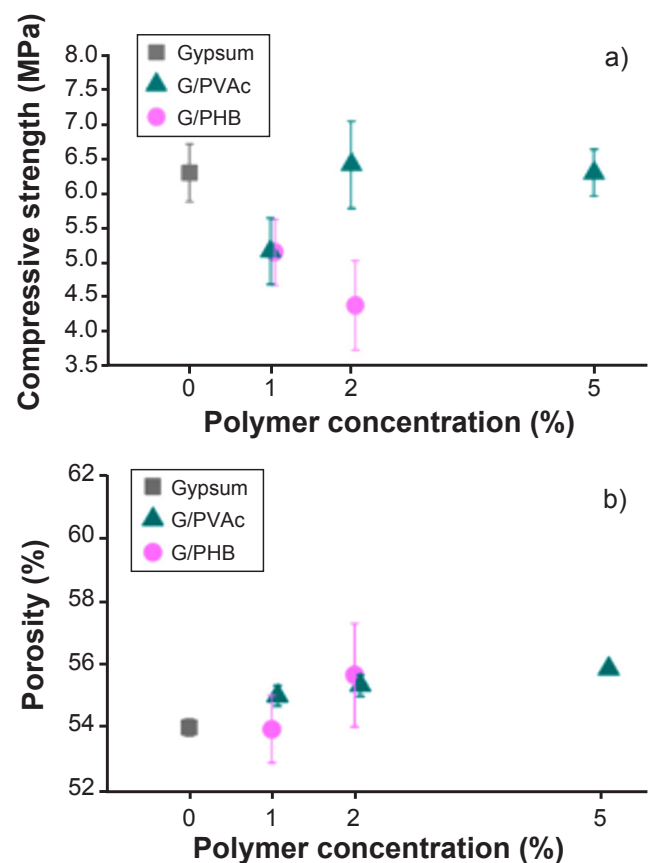


Figure 5: Compressive strength (a) and porosity (b) vs. polymer concentration of gypsum and composites fabricated by a CNC machine.

Fig. 6 provides a comparison of the compressive strengths of samples manufactured using cylindrical molds and those produced using the CNC milling machine. There was a reduction in compressive strength when both ceramic and composites underwent a subtractive manufacturing process. This observation underscored the negative influence of the machining process on the final product, as indicated by the drop in compressive strength. The combination of high porosity and residual stresses stemming from the machining process contributed to the low mechanical resistance of the materials studied during the machining process.

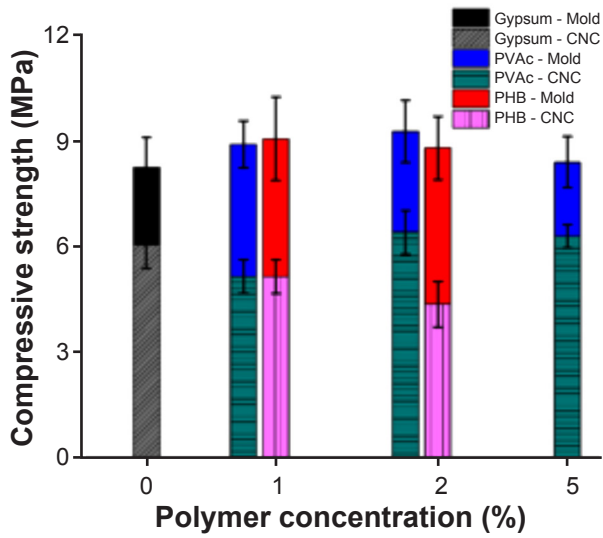
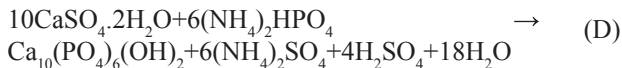


Figure 6: Comparison of compressive strength as a function of polymer concentration of samples manufactured by molding and CNC.

In Fig. 7a, the SEM image of the sample after conversion revealed the presence of granular and rough particles with various shapes. This was distinct from the morphology of dihydrate gypsum, where prismatic crystals were typically found. The EDS spectrum obtained from the sample (Fig. 7b) demonstrated the presence of the chemical elements calcium and phosphorus, which are characteristic of HAp. The conversion of gypsum into HAp is based on a process of ion diffusion within the reaction medium [2]. The reaction is described by Eq. D, indicating the exchange of sulfate ions for phosphate ions. In Fig. 7c, the XRD pattern exhibits prominent peaks at $2\theta = 25.88^\circ, 31.74^\circ, 32.18^\circ, 32.86^\circ,$ and 34.04° . These peaks aligned with those documented in the ICSD 22059 database for hydroxyapatite (HAp), and no peaks related to gypsum were observed. This confirmed a complete conversion of gypsum into HAp.



The samples produced through subtractive manufacturing were subjected to conversion into HAp with polymer by the wet method as suggested by Barbosa et al. [2]. These samples, produced using a CNC machine, are depicted in Fig. 8. They were immersed in a hydrothermal solution at 100°C for 51 h. Following this process, the samples underwent FTIR analysis. The conversion of gypsum into hydroxyapatite involved the diffusion of ions present in the reaction. Phosphate ions, stemming from the dissociation of ammonium phosphate in the medium, migrated toward the vacancies generated by the removal of sulfate ions, initially forming superficial layers of hydroxyapatite. This process continued until complete conversion was achieved after 51 h.

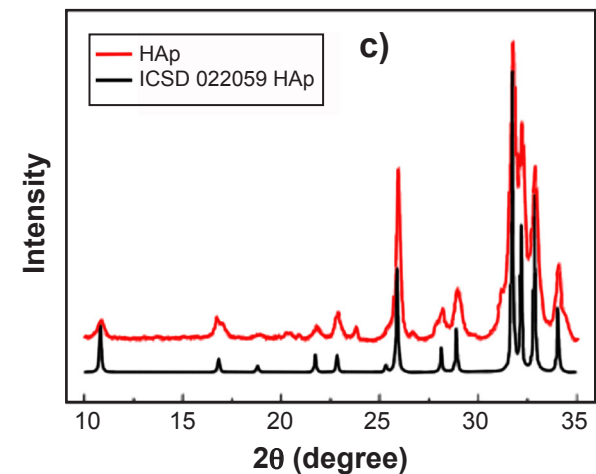
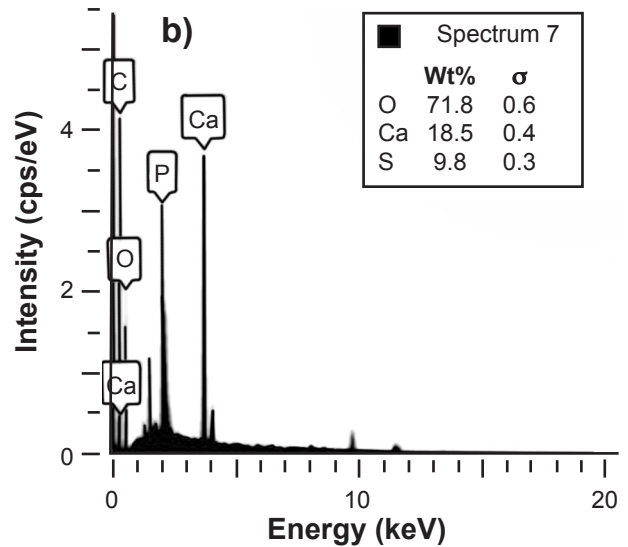
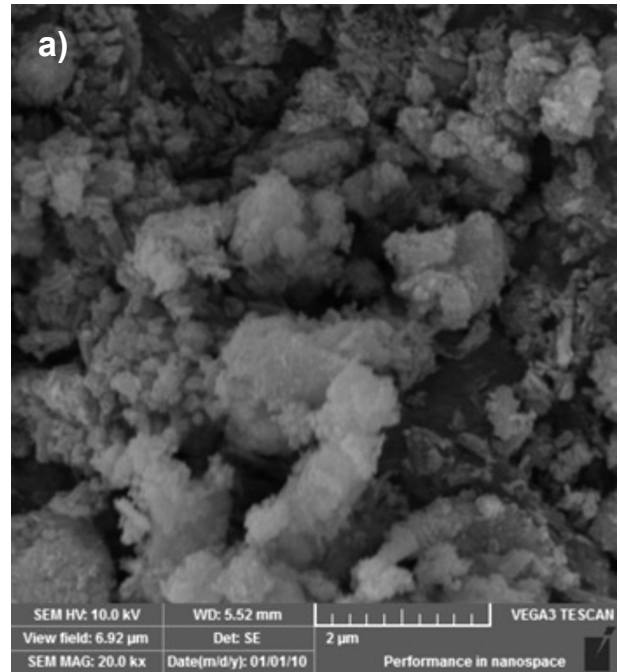


Figure 7: SEM micrograph (a), EDS spectrum (b), and XRD pattern (c) of hydroxyapatite (HAp) after conversion.



Figure 8: Images of samples: a) before conversion (gypsum/PHB); and b) after conversion (HAp/PHB).

FTIR analyses were conducted on both the surface and central regions of the bodies. In Fig. 9, the results of the conversion of gypsum into HAp without polymers are presented. In the initial analysis, after 36 h of reaction, it was evident that the reaction time was sufficient for the conversion of the material's surface (HAp-S 36 h). This is illustrated in Fig. 9, where the green curve for the material after 36 h of reaction no longer exhibited the peaks associated with sulfate ions (444, 670, 1003, and 1132 cm^{-1}). Instead, characteristic peaks of hydroxyapatite (565, 603, 1034, and 1098 cm^{-1}) related to the PO_4^{3-} group were observed. Furthermore, the emergence of the CO_3^{2-} group at 1402 cm^{-1} signified the formation of carbonated hydroxyapatite, since HAp has the capacity to adsorb CO_2 from the external environment, and carbonate ions (CO_3^{2-}) can replace the phosphate or hydroxyl groups in this compound. The analysis conducted on the central part of the sample (HAp-C 36 h) revealed that 36 h was insufficient to convert the entire body into HAp (red curve). As depicted in Fig. 9, bands related to sulfate ions were still visible in the spectrum at this stage. Complete conversion was only achieved after 51 h of the conversion process (HAp-C 51 h). In the FTIR spectrum following 51 h of conversion (blue curve), there were no longer bands

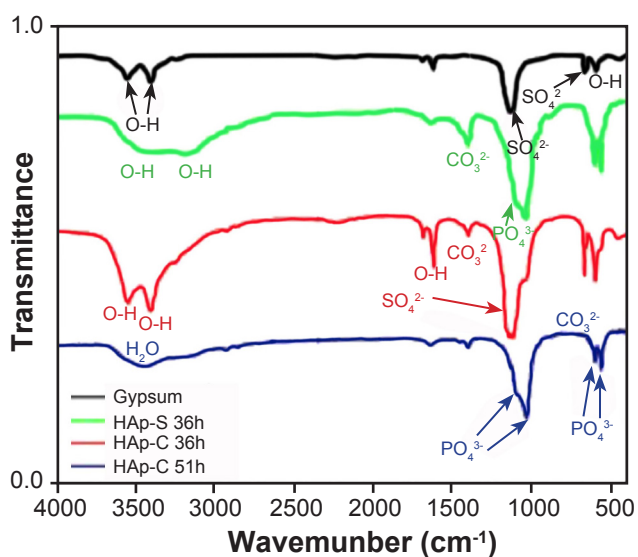


Figure 9: FTIR spectra of gypsum and central region of the sample (HAp-C) after conversion by 36 and 51 h and the surface of the sample (HAp-S) after conversion by 36 h.

related to sulfate ions, and only bands associated with HAp were identifiable. The presence of carbonate and OH groups suggested the conversion of the gypsum block into carbonated hydroxyapatite, which is commonly obtained through aqueous reactions [19]. The presence of carbonate induces structural and morphological changes in the material, offering advantages such as a reduction in the size of the crystallites, rendering them more like those found in human bone. Additionally, it enhances their solubility, making them more easily absorbable by the human body due to their proximity in composition and crystallinity to the inorganic component of human bone [20].

As depicted in Fig 10, the infrared spectrum was obtained for the HAp/PHB composite, with a sample taken from the center of the specimen, following a reaction time of 51 h. The spectrum for the HAp/PHB composite exhibited peaks associated with the PO_4^{3-} group at 564, 1034, and 1096 cm^{-1} , vibrations attributed to PHB at 1385 and 1458 cm^{-1} for the CH_3 group, and at 2353, 2923, and 2845 cm^{-1} for the CH group. Additionally, bands related to CO_3^{2-} at 1400 cm^{-1} and OH at 3432 cm^{-1} were also present. These findings confirmed the formation of hydroxyapatite reinforced with PHB in the composites. The composites made with PVAc underwent FTIR analysis after 36 h of attempting conversion to HAp. Upon analyzing the bands presented in Fig. 11, it was evident that the attempt to remove the polymer from the gypsum was not successful, as there were small traces/peaks of low intensity that were reminiscent of the polymer after the conversion of the composite into HAp; this step was necessary because PVAc is not a biomaterial. This was indicated by the presence of bands such as at 1736 cm^{-1} , which was associated with the C=O group, a characteristic band of PVAc. While bands at 566, 602, 962, and 1035 cm^{-1} related to PO_4^{3-} are characteristic of hydroxyapatite, the absorption bands at 669 and 1139 cm^{-1} are associated with SO_4^{2-} , indicating that the conversion did not occur throughout the entire block.

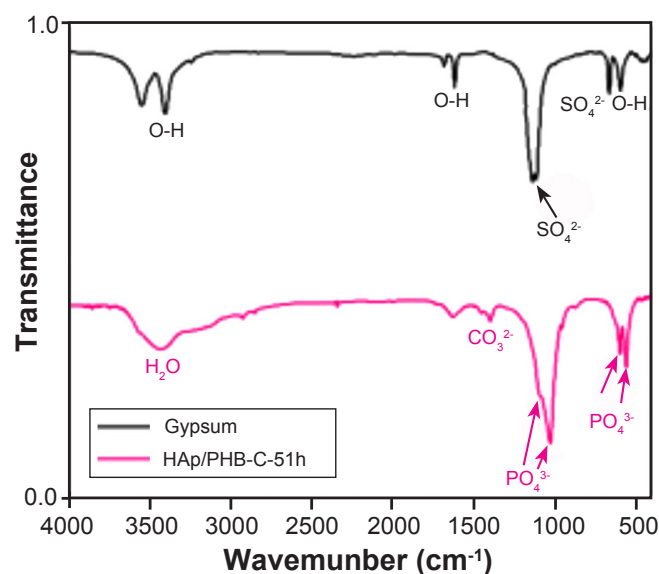


Figure 10: FTIR spectra of gypsum/PHB after 51 h conversion into hydroxyapatite compared to gypsum.

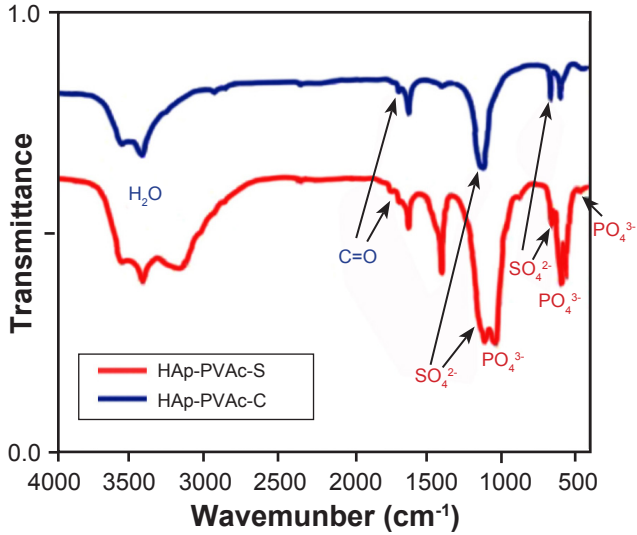


Figure 11: FTIR spectra after the conversion of gypsum/PVAc into hydroxyapatite: HAp-PVAc-S (sample’s surface) and HAp-PVAc-C (sample’s center).

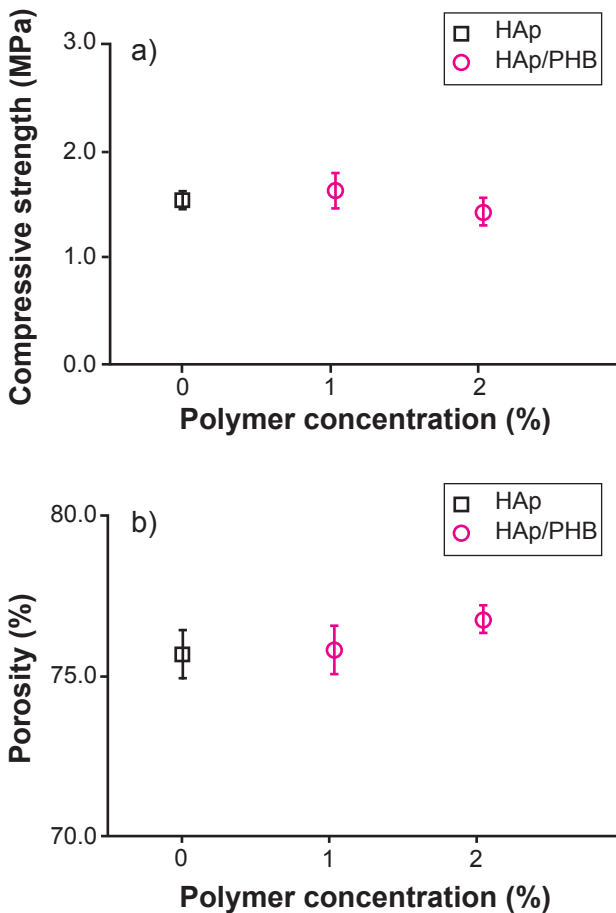


Figure 12: Compressive strength (a) and porosity (b) vs. polymer concentration of hydroxyapatite and composite samples.

The bodies that were converted into hydroxyapatite underwent mechanical compression test and porosity analysis (Fig. 12). These samples exhibited low values of

compressive strength and high porosity. The increase in porosity, as reported by Barbosa et al. [2], is a result of ion exchange, with sulfate ions being replaced by phosphate ions within the crystalline network. These phosphate ions filled the vacancies left by the removal of sulfate ions. Another contributing factor was the elimination of 1.5 water molecules present in dihydrate gypsum, which also created vacancies in the crystalline network and facilitated the incorporation of phosphate ions. After the conversion of gypsum samples into hydroxyapatite, the compressive strength reached 1.54 ± 0.08 MPa. It is important to note that the raw material had undergone a machining process, which resulted in these samples exhibiting low compressive strength values. Additionally, the addition of 1% PHB led to a slight increase in compressive strength, despite the increase in material porosity. The developed materials demonstrated their significance in biomaterial applications, as they consisted of highly porous materials with a strong resemblance to human bone, good mechanical resistance, and the ability to be prepared in complex geometries due to the subtractive manufacturing process employed with gypsum.

CONCLUSIONS

The measurement of machining forces in the turning process proved to be highly accurate, enabling the evaluation of the impact of polymeric additives on the production of ceramic bodies through subtractive manufacturing. Gypsum bodies were suitable for machining, and the forces involved in the process were remarkably low when compared to typical operations involving steel. Gypsum machining forces did not exceed 4 N, based on the cutting configurations adopted. The addition of polymers to the ceramic matrix had a notable impact on the mechanical properties. Lower polymer concentrations resulted in higher compressive strength values. In the case of PHB, when added to samples directly produced in cylindrical molds at a concentration of 1%, it led to an increase in mechanical strength, with a compressive strength of $\sigma_c = 9.1 \pm 0.4$ MPa, along with a reduction in the composite’s porosity. This concentration yielded the lowest porosity among all the samples. For the composites containing PVAc manufactured through molds, porosity had a significant influence, showing a marked increase in porosity with the increase in polymer concentration and consequently a decrease in compressive strength. However, among the samples studied, the concentration of 2% PVAc yielded the highest compressive strength, $\sigma_c = 9.3 \pm 0.3$ MPa, and porosity roughly equivalent to that of pure gypsum. Considering the low machining forces exhibited by the composites, the composite containing 2% PVAc was the most suitable for machining, as it demonstrated the highest compressive strength. It is important to note that the compressive strength of the studied materials decreased after undergoing the subtractive manufacturing process. After the conversion of the composite (gypsum/PVAc) into hydroxyapatite (HAp) and subsequent washing, it was observed through FTIR

analyses that the technique employed for polymer removal was not adequate, as the spectrum still revealed some low-intensity peaks of the polymer. Following machining, the dihydrate gypsum bodies were entirely converted into hydroxyapatite after 51 h of the wet conversion process. In the case of the gypsum/PHB composite, it was observed that the presence of polymers did not interfere with the transformation process, and hydroxyapatite/PHB was obtained within the same time frame.

ACKNOWLEDGMENT

The authors gratefully acknowledge the CAPES for financial support.

REFERENCES

- [1] R. Pastircak, A. Sladek, E. Kucharcikova, Arch. Foundry Eng. **15**, 2 (2015) 91.
- [2] A.A. Barbosa, A.V. Ferraz, N.C. Olivier, A.C.S. Dantas, Mater. Res. **17** (2014) 39.
- [3] A. Intarapadung, PNRU Acad. J. **1**, 2 (2022) 23.
- [4] G.A. Brown, K. Firoozbakhsh, T.A. DeCoster, J. Reyna Jr, JBJS **85**, suppl.4 (2003) 49.
- [5] M. Adnan, A.J. Siddiqui, S.A. Ashraf, M. Snoussi, R. Badraoui, M. Alreshidi, M. Patel, Polymers **14**, 19 (2022) 3982.
- [6] S. Park, Y.H. Yang, K.Y. Choi, Biomass Convers. Biorefin. **12** (2022) 1.
- [7] E.H. Elaiwi, A.K. Ibrahim, S.F. Al-Chalabi, A.A. Abbood, F.M. Hussein, H.H. Hussein, A.S. AL-Ridha, Mater. Today Proc. **80** (2023) 1327.
- [8] W.D. Callister Jr, D.G. Rethwisch, *Ciência e engenharia de materiais: uma introdução*, LTC, Rio Janeiro (2008).
- [9] D.W. Richerson, W.E. Lee, *Modern ceramic engineering: properties, processing, and use in design*, CRC Press (2018).
- [10] Y. Yan, T. Yu, H. Zhang, J. Song, C. Qu, J. Li, B. Yang, Crystals **11**, 12 (2021) 1494.
- [11] D. Ferraresi, *Fundamentos da usinagem dos metais*, Blucher (2018).
- [12] A.M. Dabnun, M.S.J. Hashmi, M.A. El-Baradie, J. Mater. Process. Technol. **164** (2005) 1289.
- [13] B. Hribar, N.T. Southall, V. Vlachy, K.A. Dill, J. Am. Chem. Soc. **124** (2002) 12302.
- [14] L. Portella, G. Silva, D. Costa, M. Mancini, R. Mendonça, Blucher Chem. Eng. Proc. **1**, 1 (2014) 729.
- [15] M. Su, Y. Bai, J. Han, J. Chen, H. Sun, J. Membr. Sci. **566** (2018) 104.
- [16] J. Smith, W.F. Hashemi, *Fundamentos da engenharia e ciências dos materiais*, AMGH Ed. (2013).
- [17] M. Deglurkar, D.T. Davy, M. Stewart, V.M. Goldberg, F.J. Welter, J. Biomed. Mater. Res. B Appl. Biomater. **80**, 2 (2007) 528.
- [18] B. Denkena, S. Busemann, L. Gottwik, T. Grove, A. Wippermann, Procedia Cirp **65** (2017) 70.
- [19] A.T. Teleshev, V.N. Gorshenev, M.A. Yakovleva, V.A. Fomichev, R.S. Fadeev, V.V. Minaychev, V.S. Akatov, Biomed. Eng. **52** (2018) 19.
- [20] R. Othman, Z. Mustafa, C.W. Loon, A.F.M. Noor, Procedia Chem. **19** (2016) 539.

(Rec. 11/07/2023, Rev. 28/09/2023, Ac. 21/10/2023)

